International Journal of Thermophysics, Vol. 6, No. 6, 1985

Solution of the Percus–Yevick Equation in the Coexistence Region of a Simple Fluid[1]

P. A. Monson[2] and P. T. Cummings[3]

There has been much recent interest in the behavior of integral-equation theories for the distribution functions of a fluid near the critical point and in the two-phase region. For most systems, implementation of these theories necessitates numerical solution of the integral equations. However, for two examples, the adhesive hard sphere fluid in the Percus–Yevick approximation and the hard sphere plus Yukawa tail model in the mean spherical approximation, analytical solutions of the Ornstein–Zernike equation are available. In this work we consider the comparison of results obtained via numerical methods with the analytical solution of the Percus–Yevick equation for the adhesive hard sphere fluid. This complements a recent study by us of the mean spherical approximation for the hard sphere plus Yukawa tail fluid. This allows us to examine carefully how errors arise in the numerical solutions. We examine the accuracy of numerical calculations of the critical exponents as well as the interpretation of solutions obtained in the coexistence region. We discuss the implications of this work for applications to more realistic potentials where only numerical solutions are available.

KEY WORDS: critical phenomena; integral-equation theory; Ornstein–Zernike equation; Percus–Yevick theory.

1. INTRODUCTION

An important problem in the equilibrium theory of fluids is the development of thermodynamic theories which correctly describe the nonanalyticity of the free energy at the critical point as well as accurately

[1] Paper presented at the Ninth Symposium on Thermophysical Properties, June 24–27, 1985, Boulder, Colorado, U.S.A.

[2] Department of Chemical Engineering, University of Massachusetts, Amherst, Massachusetts 01003, U.S.A.

[3] Department of Chemical Engineering, University of Virginia, Charlottesville, Virginia 22901, U.S.A.

0195-928X/85/1100-0573$04.50/0

predicting the location of the critical point and the behavior of the free energy away from the critical region. For three-dimensional systems, accurate descriptions of the critical region, such as the renormalization-group approach, are presently restricted to lattice-gas models. Although the critical exponents obtained will be the same for all other Hamiltonians in the same universality class, lattice-gas models do not provide a realistic description of the overall phase diagram of a fluid. It is a natural progression, then, to investigate the applicability to the critical region of theoretical approaches which have had some success in describing the thermodynamics outside the critical region.

Recent interest in such studies was stimulated by the work of Kozak, Luks, and collaborators on the solution of the Yvon–Born–Green equation in the Kirkwood superposition approximation (YBG-KSA) applied to the square well fluid in three dimensions [1–10]. Although it at first appeared [2–4] that the YBG-KSA theory yielded nonclassical critical exponents in close agreement with experimental values, subsequent analysis by Fishman and Fisher [6, 7] has shown that within the YBG-KSA theory, there is in fact no critical point for the square well fluid in three dimensions. Unfortunately, exact analytical solutions to this integral equation are unknown and it seems evident that the origin of the uncertainty in the behavior of the YBG-KSA theory in the critical region lies in the errors which arise from solving the integral equation numerically.

We have recently begun a study of the critical behavior of numerical solutions to a different class of integral-equation theories which arise when various closure relationships are combined with the Ornstein–Zernike (O–Z) equation. We have chosen to study this class of theories for two reasons. First, in general these theories are known to give better results than the YBG-KSA theory away from the critical region, and second, analytical solutions based on the Baxter factorization method [11] are available in two cases for Hamiltonians exhibiting critical behavior. These are the hard-core Yukawa fluid (HCYF; consisting of hard spheres with attractive interactions of the Yukawa form), for which the O–Z equation is analytically soluble in the mean spherical approximation (MSA) [12], and the adhesive hard sphere fluid (AHSF), for which the O–Z equation is analytically soluble in the Percus-Yevick (P–Y) approximation [13]. The behavior of these approximations in the critical region has been established analytically by Baxter [13] and Fishman and Fisher [14] for the AHSF in the P–Y approximation and by Cummings and Stell [15] for the HCYF in the MSA.

The essential feature of our work is the rather simple but important exercise of using a problem with an analytical solution space to evaluate a numerical method prior to using the method to study problems for which

the analytical solutions are unknown. We have recently [16] presented such a study of the HCYF in the MSA, and in the interest of brevity the reader is referred to that paper for a more extensive review of the recent studies of the critical behavior of integral-equation theories based on the O–Z equation. The present paper describes our study of the AHSF in the P–Y approximation. In Ref. 16 we noted that the behavior of the MSA at the critical point was intimately linked with the solution space in the vicinity of and inside the spinodal curve. Inside the spinodal curve there is a region where the Baxter method admits no real solutions to the MSA for the HCYF. Instead, two complex conjugate solutions arise and we presented these in Ref. 16. Similar behavior occurs in the solution of the P–Y theory for the AHSF, as we describe shortly. In the present work on the AHSF in the P–Y approximation we have introduced an innovation by relaxing the restrictions on the numerical algorithm to allow convergence to complex solutions, and such solutions have been found.

The remainder of this paper is organized as follows. In Section 2 we describe the AHSF model and review the known analytical results near the critical point. In Section 3 we outline our numerical techniques. Section 4 gives a comparison of the analytical and numerical results. Finally, in Section 5 we present our conclusions and discuss the extension of our work to other Hamiltonians for which no analytical solutions are available. A more comprehensive account of this work with details of the numerical techniques will be given elsewhere.

2. THE AHSF MODEL

The AHSF model was formulated by Baxter [13] as a limiting case of the square well potential for which the P–Y theory would have an analytical solution. The interaction potential is given by

$$\begin{aligned} \beta u(r) &= \infty, \qquad r < \sigma \\ &= -\ln[R/12\tau(R-\sigma)], \qquad \sigma < r < R \\ &= 0, \qquad r > R \end{aligned} \tag{1}$$

evaluated in the limit $R \to \sigma$ so that the Boltzmann factor becomes

$$\begin{aligned} \exp[-\beta u(r)] &= \sigma\delta(r-\sigma)/12\tau, \qquad r \leqslant \sigma \\ &= 1, \qquad r > \sigma \end{aligned} \tag{2}$$

The parameter τ can be regarded as a dimensionless measure of the

temperature of the system. A central result of Baxter's solution of the P–Y equation for this potential is the quadratic equation

$$\eta\,\lambda^2/12-[\eta/(1-\eta)+\tau]\lambda+(1+\eta/2)/(1-\eta)^2=0 \tag{3}$$

where η is the volume fraction of spheres in the system and λ is a parameter which determines the magnitude of the delta function contribution to the pair distribution function at $r=\sigma$. Knowledge of $\lambda(\eta,\tau)$ is sufficient to determine the contribution of the attractive interactions to the thermodynamic properties. It can be shown that the compressibility equation of state has a critical point given by

$$\begin{aligned}\tau_c&=(2-\sqrt{2})/6\approx 0.09763\\ \eta_c&=(3\sqrt{2}-4)/2\approx 0.1213\\ \rho_c\sigma^3&=6\eta_c/\pi\approx 0.2317\end{aligned} \tag{4}$$

The critical exponents have classical values. However, the critical isotherm displays a large asymmetry with respect to the critical point which is caused by nonclassical scaling functions [14]. Some important features of the analytical solution space of the approximation are illustrated in Figs. 1 and 2. Figure 1 shows the three regions of the solution space. Inside region I, the solutions are real, the inverse compressibility is positive, and the correlations decay at large separations. The boundary between region I and region II is the spinodal curve. In region II the solutions are real and the inverse compressibility positive, but the total correlation function $h(r)$ diverges at large r. In region III there are no real solutions, but by analytic continuation two complex conjugate solutions may be found. The point where the curves which separate the regions meet coincides with the critical point. This contrasts with the case of the HCYF-MSA problem [16], where the region of complex solutions does not extend up to the critical temperature. Figure 2 shows several isotherms of the inverse compressibility at the critical temperature and subcritical temperatures. The two singularities in each subcritical isotherm occur at the boundaries of region III. Thus between these two points the curve gives the real part of the inverse compressibility. On the vapor side, however, the region III extends beyond the locus of zeros of the real part of the bulk modulus. Thus there is no spinodal curve in the true sense on the vapor side of the coexistence region. Notice also that on the liquid side there are two zeros in the bulk modulus. The limit of stability of the liquid corresponds to a point of inflection in the pressure. The zero of the bulk modulus corresponding to a pressure minimum lies inside the region of complex solutions.

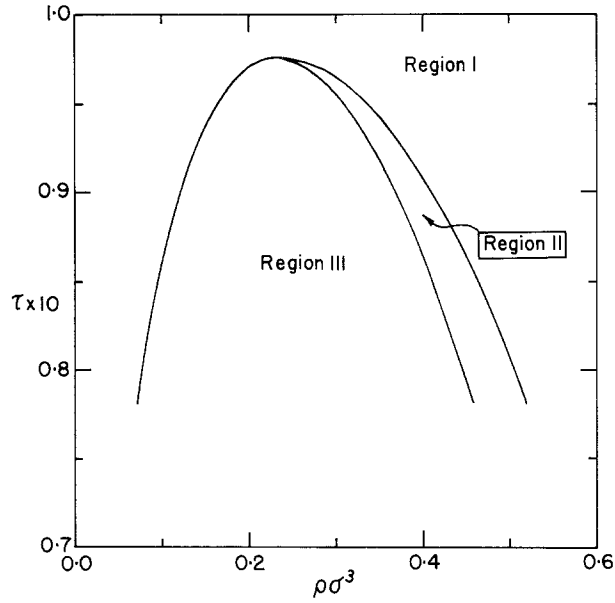

Fig. 1. The three regions of the solution space found analytically for the AHSF in the P–Y approximation. Inside region I, the solution is real, the compressibility is positive, and the correlation functions decay at large r. The boundary between region I and region II is the spinodal curve. In region II, the solution is real, and the compressibility positive. However, $h(r)$ diverges at large r. Inside region III, the solution is complex, yielding both real and imaginary parts for the distribution functions and thermodynamic properties.

In a number of respects, then, the AHSF in the P–Y approximation exhibits what might be regarded as anomalous behavior. Nevertheless, it is the only one of two cases (the other being the Kac model [17] of a hard core plus an infinitely weak and long-ranged attraction) for which the analytic solution of the P–Y approximation is known for a Hamiltonian exhibiting a vapor–liquid transition. For this reason it is instructive to examine the extent to which the numerical techniques can be used to elucidate the solution space.

3. NUMERICAL SOLUTIONS

In our numerical solutions we have used two methods. For temperatures above critical we have used the method of Gillan [18]. However, we found that it was difficult to achieve convergence reliably at low tem-

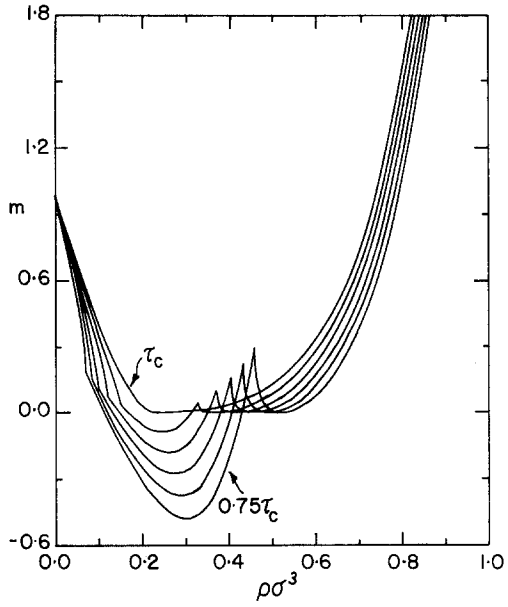

Fig. 2. The dimensionless inverse compressibility $m = 1/kT\,\partial P/\partial\rho$ for the AHSF obtained from the analytical solution. Six isotherms are illustrated: $\tau/\tau_c = 1.0$, 0.95, 0.9, 0.85, 0.8, and 0.75. Since the inverse compressibility is complex between the two singularities, only the real part is shown. Notice the asymmetry of the critical isotherm.

peratures with this method. We therefore used a full Newton–Raphson technique for the subcritical temperatures. Such a technique was first used by Watts [19] in a study of the P–Y and hypernetted chain theories for the Lennard–Jones 12-6 potential. Use of this technique has also made it straightforward to admit convergence to complex solutions. Ironically, the features of the AHSF model which render it analytically soluble in the P–Y approximation create some difficulties for the numerical solution. These come principally from the long-ranged contributions in Fourier space which arise from the delta function contribution to the direct correlation function. These contributions are easily identified and their contribution to the Fourier transforms may be handled analytically.

The numerical techniques used in the present work are both based on the O–Z equation in Fourier space. This has the advantages that the convolution in the O–Z equation is very simply evaluated and use of the fast Fourier transform further reduces the computation time for this step by an

order of magnitude. However, in evaluating the Fourier transforms one is perforce limited to the use of a finite cut off in r-space. This of course leads to errors at the critical point and on the spinodal curve, and these errors are an important source of discrepancy between the numerical and the analytical solutions as was found in the case of the MSA for the HCYF model. One possible approach to removing such errors is to consider numerical methods which do not require such a truncation. Some numerical methods based upon the Baxter factorization technique which fulfill this requirement are discussed in Ref. 16. We are currently investigating these methods and the results will be reported in a future publication.

4. RESULTS

We now consider the comparison of our numerical solutions with the analytical results, beginning with the behavior of the system near the critical point. We focus on the values of the critical exponents δ and γ, which control the divergence of the isothermal compressibility along the critical isotherm and critical isochore, respectively. It is known from the

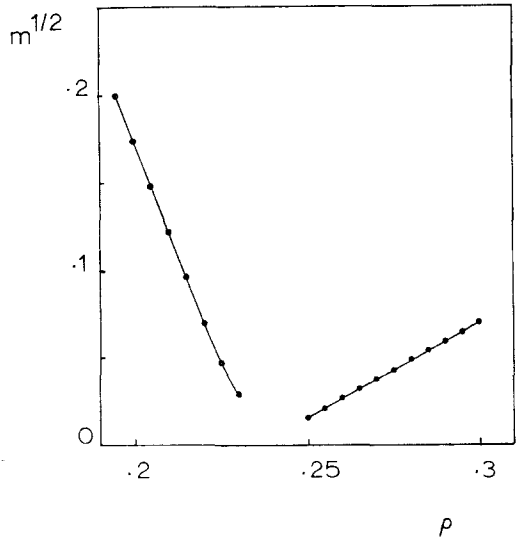

Fig. 3. The square root of the dimensionless inverse compressibility is shown as a function of the density from the numerical results at $\tau = 0.097475$, which is very close to the critical isotherm. The results were obtained using $\Delta r = 0.025\sigma$ and $r_c = 25.6\sigma$.

work of Baxter [13] that these exponents have the classical values ($\delta = 3$, $\gamma = 1$) for the AHSF in the P–Y approximation. We have made a number of comparisons of isotherms of the inverse compressibility in the critical region from the numerical and analytical results. On the critical isotherm such a plot should be quadratic near the critical density. We find fairly large differences between the analytical and the numerical results near the critical density. For example, the isotherm at $\tau = 0.0976$ appears slightly subcritical in the analytical solution but is clearly supercritical in the numerical solution with the given parameters. We have made calculations with other solution parameters and have found that the agreement between the numerical and the analytical solutions is improved as the r-space cutoff is increased, as might be expcted. However, increasing the cutoff from 12.8σ to 25.6σ does not significantly effect the results at $\tau = 0.0976$. This indicates that very much larger values than these would be needed in order to bring the analytical and numerical solutions into agreement. Figure 3 shows the numerical results for the square root of the inverse compressibility at a

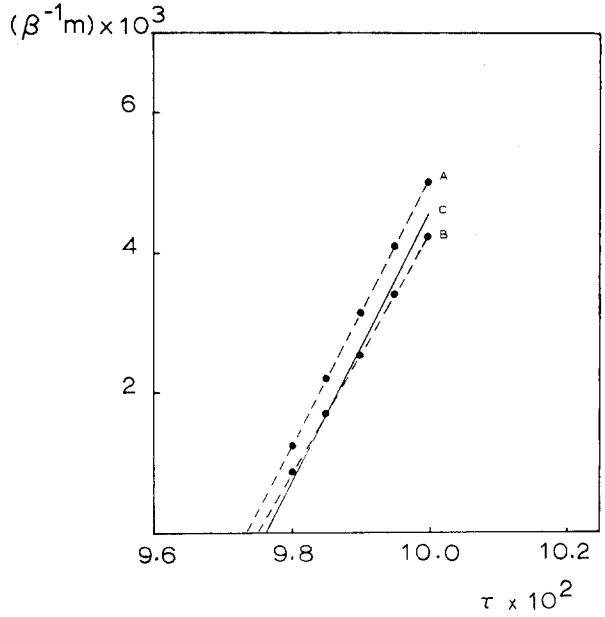

Fig. 4. The inverse compressibility as a function of τ on isochores close to critical. The dashed lines give the numerical results for two densities which bound the critical density, and the solid line gives the analytical results on the critical isochore. The letters A, B, and C denote the value of $\rho\sigma^3$: A, 0.23; B, 0.24; and C, 0.2317. The numerical results were obtained using $\Delta r = 0.025\sigma$ and $r_c = 25.6\sigma$.

temperature very close to critical, obtained using an r-space cutoff of 25.6σ. Apart from very close to the critical density on the low-density branch, linear behavior is clearly established. We can therefore conclude that a value of $\delta = 3$ may be reasonably safely deduced from the numerical solutions. A reasonable estimate of the critical point from the numerical solutions would be $\rho_c = 0.235 \pm 0.002$ and $\tau_c = 0.0975 \pm 0.0002$.

A value of $\gamma = 1$ implies that on the critical isotherm, a plot of the inverse compressibility versus τ should be linear. Figure 4 shows such a plot from our numerical solutions at two densities which bound the critical density together with the analytical results on the critical isochore. The plots demonstrate that a value of $\gamma = 1$ may be deduced from the numerical solutions.

We now turn to a consideration of the solutions in the two-phase region. As mentioned earlier, in these studies we have used a Newton–Raphson technique in our numerical work and have allowed con-

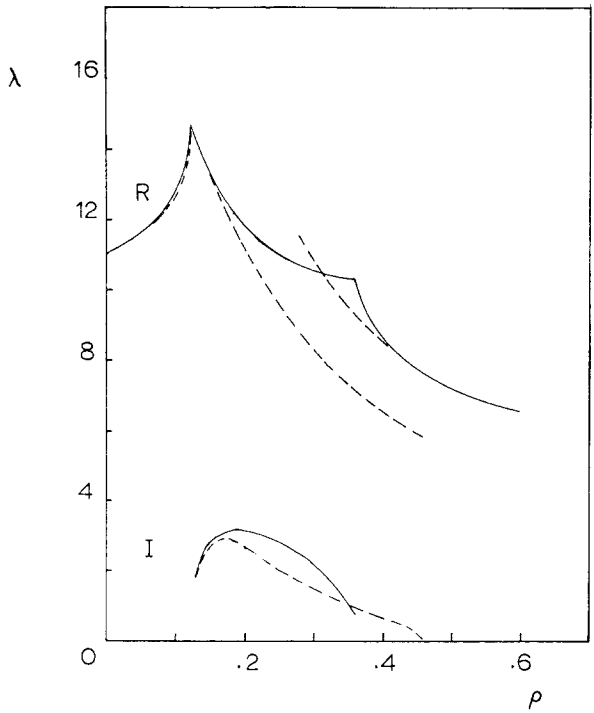

Fig. 5. The parameter λ on the isotherm at $\tau = 0.09$. The solid line gives the analytical results, and the dashed line the numerical results. The numerical results were obtained using $\Delta r = 0.05\sigma$ and $r_c = 6.4\sigma$.

vergence to complex solutions. In order to keep the dimension of the Jacobian within reasonable limits, we used a grid size, Δr, of 0.050 and an r-space cutoff of 6.4σ in these calculations. Figure 5 shows a plot of the parameter λ as a function of the density at $\tau = 0.09$ from the analytical solution and numerical solutions. Notice that between the cusps, which occur at the boundary of region III in Fig. 1, λ has both real and imaginary parts. The agreement between the numerical and the analytical solutions is very good at a low density and at the highest densities. However, at intermediate densities the agreement is poor. This is not surprising since in regions II and III in Fig. 1, the analytical results indicate that $h(r)$ becomes divergent at large r as the density increases. Such behavior cannot be reproduced in our numerical work because we use a finite cutoff in r-space. Equation (3) shows that only two solutions (which in region III are complex conjugates) for λ are admitted in the analytical solution. In contrast, the numerical procedure gives rise to a multiplicity of solutions. We have found two pairs of complex conjugate solutions and one real solution using the numerical method, and we have no reason to assume that other solutions are not present. Results from one of the complex solutions and the real solution are illustrated in Fig. 5. There does not seem to be a con-

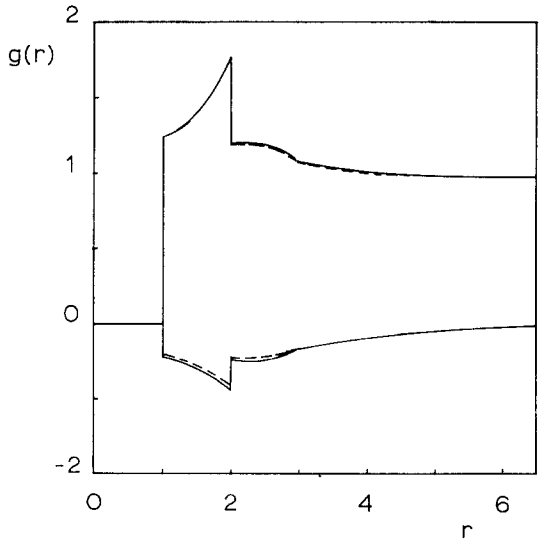

Fig. 6. The radial distribution function at $\rho\sigma^3 = 0.14$ and $\tau = 0.09$. The solid line gives the analytical results, and the dashed line the numerical results. The numerical results were obtained using $\Delta r = 0.05\sigma$ and $r_c = 6.4\sigma$. The top curves are the results for the real part of the radial distribution function, and the bottom curves are those for the imaginary part.

tinuous path of numerical solutions through the two-phase region. This may be related to the asymmetry of the model with respect to the critical point. The multiplicity of numerical solutions would seem to arise from the use of a finite r-space cutoff in the numerical work. Mier y Terán et al. [20] found three real solutions to the P–Y theory for the Lennard–Jones potential in the same region of the phase diagram using an algorithm based on a finite r-space cutoff, although complex solutions were not admitted and they were able to find a continuous path of solutions through the two-phase region.

Figure 6 shows a comparison of the analytical and numerical results for $g(r)$ at $\tau = 0.09$ and $\rho = 0.14$ which is a state just inside region III in Fig. 1 on the vapor side. The agreement is good except for a slight difference in the imaginary part. We have made such comparisons at a higher density ($\rho = 0.3$) and find that the agreement is very poor. The analytic solution at this density yields two complex conjugate solutions. Both the real and the imaginary parts of $g(r)$ are long ranged and oscillatory. Clearly, the numerical solutions based on a finite r-space cutoff cannot reproduce the behavior of the analytical solution. As mentioned above a multiplicity of solutions is found: two pairs of complex conjugate solutions and one real solution.

5. SUMMARY AND DISCUSSION

The results of this paper may be summarized as follows. Numerical solutions of the P–Y equation for the AHSF model using the Gillan method can give a quite accurate picture of the compressibility-equation critical point. The critical exponents δ and γ are correctly deduced to have classical values and the severe asymmetry of the critical isotherm is reflected in the numerical results. We therefore conclude that careful numerical work should be able to elucidate such features of the critical behavior of other Hamiltonian models in the P–Y approximation when analytical solutions are not available.

We have shown that the complex solutions to the P–Y equation which may be obtained by analytic continuation of Baxter's solution into region III in Fig. 1 can also be obtained by numerical methods. However, good agreement between the solutions is obtained only at the lower densities, where the distribution functions from the analytical solution do not diverge at large r. The preliminary studies of these questions in the present paper raise some intriguing questions concerning the behavior of the P–Y equation in the two-phase region. For example, it would be interesting to know if the low-temperature solution space of the AHSF in the P–Y

approximation is the same as that for more realistic Hamiltonians. Some evidence supporting this comes from the work of Watts [19] on the 12–6 potential, but only real solutions were considered. Another question is that of the relationship between the closure approximation and the solution space. Indeed the results of this paper and of Ref. 16 show significant differences between the MSA for the HCYF and the P–Y theory for the AHSF.

We hope to investigate these matters in future research.

ACKNOWLEDGMENTS

PTC gratefully acknowledges the support of this research by the Camille and Henry Dreyfus Foundation through the award of a grant for New Faculty in the Chemical Sciences. The authors are grateful to the Engineering School and Computing Center at the University of Massachusetts and the Center for Computer Aided Engineering at the University of Virginia for provision of computing facilities.

REFERENCES

1. W. W. Lincoln, J. J. Kozak, and K. D. Luks, *J. Chem. Phys.* **62**:2171 (1975).
2. K. U. Co, J. J. Kozak, and K. D. Luks, *J. Chem. Phys.* **64**:2197 (1976).
3. K. Green, K. D. Luks, and J. J. Kozak, *Phys. Rev. Lett.* **42**:985 (1979).
4. K. Green, K. D. Luks, E. Lee, and J. J. Kozak, *Phys. Rev. A* **21**:356 (1980).
5. G. L. Jones, J. J. Kozak, E. Lee, S. Fishman, and M. E. Fisher, *Phys. Rev. Lett.* **46**:795 (1981).
6. S. Fishman, *Physica (Utrecht)* **A109**:382 (1981).
7. M. E. Fisher and S. Fishman, *J. Chem. Phys.* **78**:4227 (1983).
8. K. A. Green, K. D. Luks, G. L. Jones, E. Lee, and J. J. Kozak, *Phys. Rev. A.* **25**:1060 (1982).
9. G. L. Jones, E. Lee, and J. L. Kozak, *Phys. Rev. Lett.* **48**:447 (1982).
10. G. L. Jones, E. Lee, and J. J. Kozak, *J. Chem. Phys.* **79**:459 (1983).
11. R. J. Baxter, *Austr. J. Phys.* **21**:563 (1968).
12. E. Waisman, *Mol. Phys.* **25**:45 (1973). This paper actually uses a related analysis due to M. S. Wertheim, *J. Math. Phys.* **5**:643 (1964). However, the Baxter method may also be used. See P. T. Cummings and E. R. Smith, *Mol. Phys.* **38**:997 (1979).
13. R. J. Baxter, *J. Chem. Phys.* **49**:2770 (1968).
14. S. Fishman and M. E. Fisher, *Physica (Utrecht)* **A108**:1 (1981).
15. P. T. Cummings and G. Stell, *J. Chem. Phys.* **78**:1917 (1983).
16. P. T. Cummings and P. A. Monson, *J. Chem. Phys.* **82**:4303 (1985).
17. M. Kac, G. E. Uhlenbeck, and P. C. Hemmer, *J. Math. Phys.* **4**:216 (1963).
18. M. J. Gillan, *Mol. Phys.* **38**:1781 (1979).
19. R. O. Watts, *J. Chem. Phys.* **48**:50 (1968).
20. L. Mier y Terán, A. H. Falls, L. E. Scriven, and H. T. Davis, *Proceedings of the 8th Symposium on Thermophysical Properties*, J. V. Sengers, ed. (American Society of Mechanical Engineers, New York, 1982), p. 45.